Desalination and Water Treatment
www.deswater.com

doi: 10.5004/dwt.2019.23781

151 (2019) 322–331
May

Capture and adsorption behavior of iodine by edible γ-CD-MOFs

Haiyang Yu, Xinchen Lin, Xiyuan Yang, Yifan He, Heda Guan, Donglei Zou, Yangxue Li*

Key Lab of Groundwater Resources and Environment, Ministry of Education, Jilin University, 2519 Jiefang Road, Changchun 130021, China, Tel./Fax: +86 431 88498251; emails: yangxueli@jlu.edu.cn (Y. Li), 150216264@qq.com (H.Y. Yu), 3507543118@qq.com (X.C. Lin), aiyan-zhanhuo@163.com (X.Y. Yang), 13644410977@163.com (Y.F. He), zhiliu1980@gmail.com (H.D. Guan), 2917758@qq.com (D.L. Zou)

Received 2 August 2018; Accepted 12 January 2019

ABSTRACT

The capture and storage of radioactive iodine (^{129}I or ^{131}I) generated from the extensive use of nuclear energy has become a hotspot. In our work, we exerted the edible γ-CD-MOFs with high specific surface area large cavities and plenty of hydroxyl functional groups to iodine capture and adsorption process. The most significant parameters including dosages, contact times, adsorbate concentrations and temperatures were explored. The external adsorption behavior was analyzed by kinetic analysis as well as thermodynamic analysis, and the internal mechanism was investigated in detail. The results showed that the adsorption obey the pseudo-second order kinetic model. The maximum gas iodine uptake of 104 wt% was obtained and the maximum liquid adsorption capacity was as high as 449.71 mg/g at 298 K estimated by the Langmuir isotherm model. Additionally, the negative values of ΔG and the positive values of ΔH and ΔS at all temperatures, suggested that the spontaneous and endothermic nature of the iodine adsorption by γ-CD-MOFs.

Keywords: γ-CD-MOFs; Iodine; Adsorption; Kinetic analysis; Thermodynamic analysis

1. Introduction

Iodine is an indispensable trace element in the human body. However, excess iodine and its radioactive isotopes will pose a threat to human health, i.e., it could damage thyroid function and further may lead to an increase in thyroid cancer. The radioactive iodine is mainly derived from the release of nuclear accidents, among which containing 16 kinds of output data, namely I^{123}, I^{125} and $I^{127–140}$ [1]. Major accidents in recent years generally including the Chernobyl nuclear disaster in Ukraine in 1986, the Davis-Bose reactor accident in the United States in 2002, the Mihama nuclear power plant accident in Japan in 2004, Fukushima and Daiichi nuclear power plant accident in Japan in 2011, etc. All above had great effects on the environment and then caused the variation of plants and animals [2–4]. Therefore, a surge to explore effective measures of controlling radioactive iodine pollution has witnessed in recent decades.

Up to now, the methods of iodine removal have been mainly focused on the adsorption technology, which is the most popular and effective approach due to its attractive advantages such as simple operation, little equipment investment cost and energy consumption, no production of toxic intermediates [5,6]. The traditional porous adsorbents often used to handle iodine pollution including silica gel, activated alumina, activated carbon, molecular sieve, etc [7,8]. However, there are some shortcomings of the traditional adsorbents evident in the low adsorption capacity, easy-lost activity and so on. For example, the adsorption efficiency of the conventional silver-based zeolite used to capture radioactive iodine is low because of the limited available surface; besides, the cost is high and adverse environmental impact is great due to the composition of silver [9]. Hence, developing new adsorbents with high adsorption capacity, low cost and strong adaptability is still desirable.

* Corresponding author.

Porous metal–organic frameworks (MOFs), which mainly formed from the inorganic metal clusters and organic ligands, have been rapidly developed as a new type of solid adsorbents by virtue of high specific surface areas, large porosities, adjustable pore sizes and structures and devisable adsorption sites [10–18]. In recent years, MOFs have been employed for addressing environmental issues to decontaminate various toxic and hazardous substances involving lead ions, hexavalent chromium ions, organophosphorus, nitrobenzene and antibiotics [19]. However, the utilization of MOFs to remove iodine and investigation of the adsorption behavior remain to be further developed.

Among the numerous MOFs, the edible gamma-cyclodextrin MOFs (γ-CD-MOFs) with body-centered cubic structures, which are constructed by potassium ions and γ-CD, have become highly sought-after [20–23]. Particularly, the organic linker of γ-CD, which comprised of eight asymmetric α-1,4-linked D-glucopyranosyl residues, is a symmetrical cyclic oligosaccharide produced enzymatically from starch. Consequently, the γ-CD-MOFs were endowed with large spherical pores of 17 Å bearing plenty of hydroxyl functional groups [24,25]. Judging from the characteristics of high specific surface areas, large cavities and polyhydroxy functional groups, herein, we adopted the γ-CD-MOFs as efficient adsorbents for the capture and adsorption of iodine. The results were characterized by powder X-ray diffraction (PXRD), X-ray photoelectron spectroscopy (XPS) and Fourier Transform Infrared Spectra (FT-IR). In addition, the adsorption kinetics, adsorption isotherms and thermodynamics of iodine by the γ-CD-MOFs were studied.

2. Experimental setup

2.1. Materials

All chemicals (gamma-cyclodextrin, potassium hydroxide, methanol and iodine) were purchased from commercial suppliers and used without further purification unless otherwise noted.

2.2. Instruments and characterization

The Fourier Transform Infrared Spectra (FT-IR) were measured on a Nicolet Nexus 410 infrared spectrometer spectrum instrument using the KBr method at the wavelength from 4,000 to 400 cm^{-1}. The powder X-ray diffraction (PXRD) was performed by a Riguku D/MAX2550 diffractometer using *CuKα* radiation, 40 kV, 200 mA with scanning rate of 4°/min. The nitrogen adsorption isotherm was measured on an Autosorb iQ2 adsorptometer, Quantachrome Instruments. The X-ray photoelectron spectroscopy (XPS) was recorded on a ESCALAB 250Xi X-ray photoelectron spectroscopy. The optical absorption spectra were recorded using UV–Vis spectrophotometer (Varian Cary 3 Bio, Australia).

2.3. Synthesis of γ-CD-MOFs

The γ-CD-MOFs were synthesized according to the previous literature (Fig. 1) [25]. Specifically, (1) A mother solution of γ-Cyclodextrin (324 mg) in 200 mM KOH aq. (10 mL) was placed in a glass vessel; (2) 6 mL CH_3OH was allowed to vapor-diffuse into the foregoing solution at room temperature for incubating the colorless cubic single crystals.

2.4. Uptake of iodine

The solid iodine adsorption experiments were performed as follows: (i) the γ-CD-MOFs were placed into a sealed vessel, which filled with nonradioactive iodine vapor at 353 K and atmospheric pressure; (ii) after a period of time, the anterior vessel was cooled down to room temperature and weighed. The uptake of iodine for γ-CD-MOFs was calculated as the following formula:

$$\alpha = \frac{m_2 - m_1}{m_1} \times 100\% \quad (1)$$

where α represents the iodine uptake, m_1 and m_2 represent the quality of γ-CD-MOF samples before and after adsorption of iodine.

2.5. Adsorption of iodine

Adsorption of iodine by the γ-CD-MOFs was conducted with batch experiments. The γ-CD-MOFs (10 mg) were fit in the iodine/hexane solution (50–700 mg/L, 10 mL) and held for a period of time. Then the absorbance of supernatant was measured at a wavelength of 525 nm by UV-vis at various time intervals with a calibration plot (Fig. S1).

The removal efficiency (E, %) and the amount of iodine adsorbed q_e (mg/g) were given according to the formulas [26]:

$$q_e = \frac{(C_0 - C_e)V}{m} \quad (2)$$

$$E(\%) = \frac{C_0 - C_e}{C_0} \times 100\% \quad (3)$$

where C_0 (mg/L) and C_e (mg/L) represent the initial concentration and equilibrium concentration of iodine in the solution, respectively; m represents the mass of adsorbent used (g); V represents the volume of solution used (L).

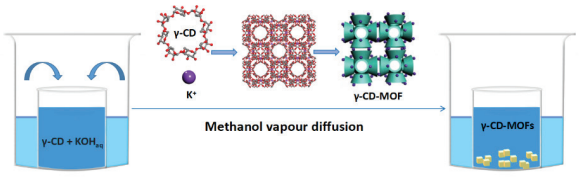

Fig. 1. Synthesized producer of γ-CD-MOFs.

3. Results and discussion

3.1. Iodine capture

The PXRD pattern of γ-CD-MOFs was matched with the previously reported result predicted from the single crystal crystallographic data, which is in line with the pure phase of the obtained samples (Fig. S2). The N_2 adsorption–desorption isotherms (Fig. 2) of the γ-CD-MOFs used in this study defined a Brunauer-Emmett-Teller (Langmuir) surface area of 374.8 (485.4) $m^2\ g^{-1}$. To investigate the ability of γ-CD-MOF materials for iodine enrichment, the capture experiment of excess iodine vapor by γ-CD-MOFs was conducted in a closed system at 353 K and ambient pressure. With the passage of time, the color of the γ-CD-MOFs changed from colorless to dark brown, and the uptake quality was calculated by the gravimetric method. As shown in Fig. 3, the adsorption rate increased rapidly in the first 2 h, then significantly reduced from 2 to 5 h, and gradually became even after 5 h, indicating that

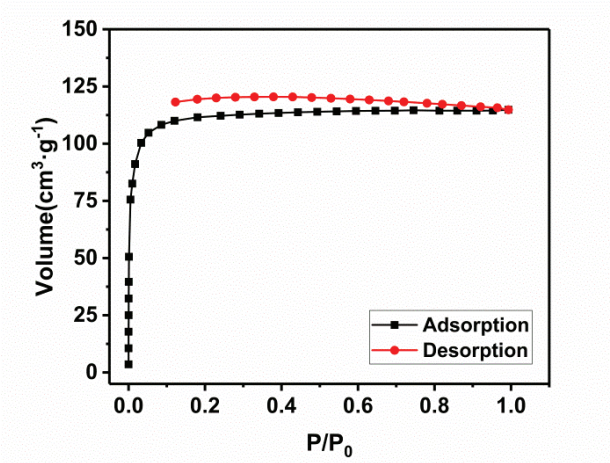

Fig. 2. N_2 adsorption–desorption isotherms for the γ-CD-MOFs.

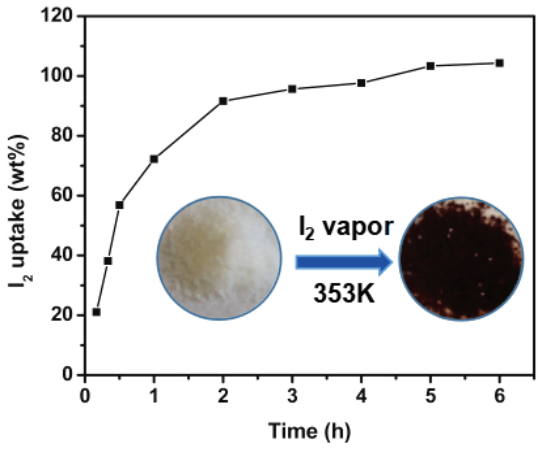

Fig. 3. Gravimetric uptake of non-radioactive iodine by γ-CD-MOFs as a function of time at 353 K. Inset photographs showing the color change when γ-CD-MOFs were exposed to iodine vapor 5 h.

the adsorption reached equilibrium with a saturated iodine loading of 104 wt%. With this vapor uptake value of iodine, γ-CD-MOFs could far exceed the commercial activated carbon as high as 3.4 times (Table S1). The efficient iodine adsorption performance of γ-CD-MOFs may arise from two aspects: (a) the high specific surface area characteristics and large cavities may be propitious to improve the adsorption capacity of iodine by γ-CD-MOFs; (b) the abundant hydroxyl groups could enhance the affinity between the γ-CD-MOFs and iodine molecules.

The XPS spectrum of the iodine-loaded samples (named as I_2@γ-CD-MOFs) washed with ethanol three times is shown in Fig. 4(a). For I_2@γ-CD-MOFs, both I 3d 3/2 peak and I 3d 5/2 peak could be decomposed into two components of I_2 (631.6, 629.8 eV) and I_3^- (620.1, 618.4 eV), respectively. The result demonstrated the coexisting of iodine and polyiodide states (I_3^-), suggesting the chemisorption and physisorption occur simultaneously. This phenomenon could be contributed to the strong affinity to iodine molecular presented by the hydroxy affinity centers in γ-CD-MOFs; this is, I_2 species could be transformed into I_3^- with polyhydroxy skeleton of γ-CD-MOFs through the transfer of electron from the O atom to I atom charge-transfer effect [7,27].

Furthermore, when comparing the FT-IR spectra of I_2@γ-CD-MOFs to parent γ-CD-MOFs, we found that the O–H stretching vibrations at 3,387 cm^{-1} red-shifted toward to 3,374 cm^{-1}, implying the noncovalent interactions between O–H groups of γ-CD-MOFs with iodine (Fig. 4(b)). In another word, the FT-IR spectrum as well as XPS spectrum provided the solid evidence for the existence of the charge-transfer (CT) interactions between the O–H units electron donor and iodine acceptor [4,28]. Thus, the γ-CD fragments in the γ-CD-MOF skeleton might play a crucial role in the iodine capture.

3.2. Iodine adsorption

3.2.1. Effect of adsorbent dose

In a batch system, γ-CD-MOF dosages varied from 0.25 to 3g/L were tested to evaluate the optimal value for a fixed concentration of iodine at 100 mg/L. As shown in Fig. 5, the E increased from 23.23% to 98.25%, while the q_e reduced from 175 to 35 mg/g with the increase of γ-CD-MOF dosages. This mechanism could be explained as: the increasing amount of γ-CD-MOFs produced the raising of contacting surface area and binding sites for iodine adsorption, resulting in the improving of removal efficiency; on the other hand, the adsorptive capacity dropped because of the decreased amount of iodine exposed to unit weight of γ-CD-MOFs. After weighing, the optimum adsorbent dosage was fixed at 1 g/L, and then it was used for the subsequent experiments.

3.2.2. Effect of contact time and initial concentration

The impact of contact times and initial concentrations of the solution on the absorption of iodine by γ-CD-MOFs were conducted at room temperature. As shown in Fig. 6(a), the color of the solution gradually decreased from dark pink to almost colorless after 12 h; in contrast, the γ-CD-MOFs

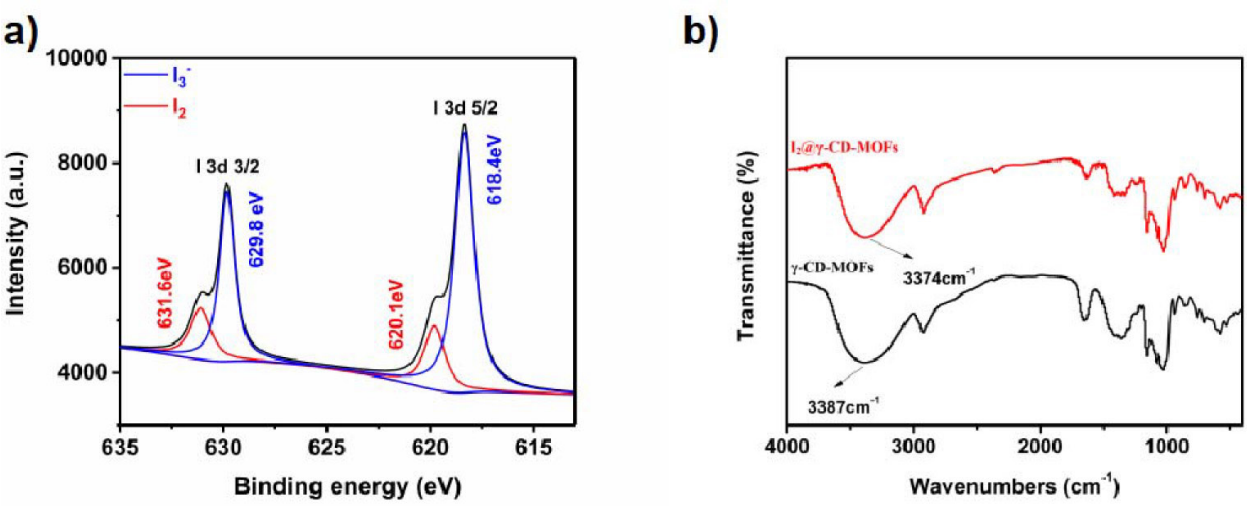

Fig. 4. (a) XPS spectrum of I_2@γ-CD-MOFs (b) FT-IR spectra of γ-CD-MOFs and I_2@γ-CD-MOFs.

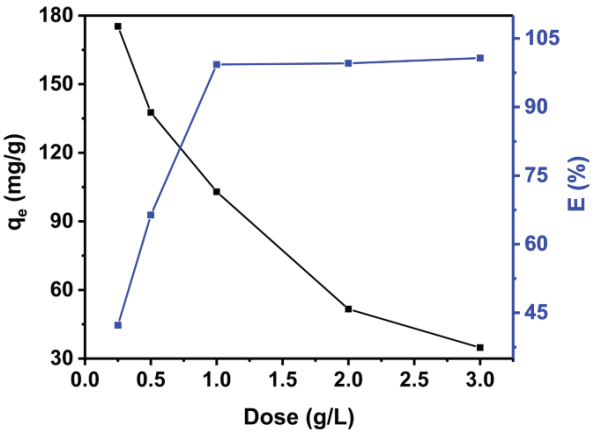

Fig. 5. Variation in the removal efficiency E and adsorptive capacity q_e of γ-CD-MOFs as a function of adsorbent dose.

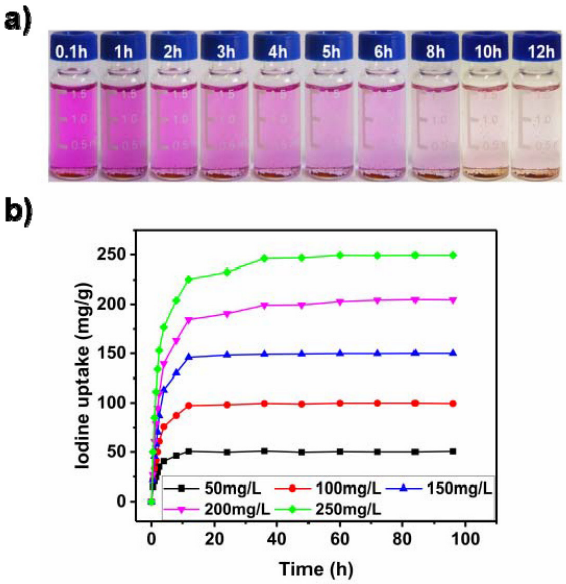

Fig. 6. (a) Photographs showing the visual color change of iodine adsorption by γ-CD-MOFs. and (b) Kinetics of iodine adsorption by γ-CD-MOFs in n-hexane solution at different concentrations (50–250 mg/L) at T = 298 K.

turned from white to purple. As expected, the longer the contact time as well as the larger the initial iodine concentration was, the higher the iodine adsorption amount was. Overall, the equilibrium of iodine adsorption by γ-CD-MOFs happened at 12 h (Fig. 6(b)). At first, a large number of the hydroxyl active sites were exposed on the surface of γ-CD-MOFs, the adsorption amount sharply raised; then, when the active sites were gradually occupied, the adsorption amount slowly paced down; finally, it reached the saturation. When the initial concentration ranged from 50 to 250 mg/L, the corresponding maximum adsorption amounts and removal efficiencies of iodine by γ-CD-MOFs were 50.00 mg/g and 100%, 98.23 mg/g and 98.23%, 147.24 mg/g and 98.13%, 190.59 mg/g and 95.30% and 232.94 mg/g and 93.18%, respectively. Obviously, the effective collision probability between γ-CD-MOFs and iodine raised with the increase of initial concentration of iodine, bringing the enhanced adsorption capacity.

3.2.3. Adsorption dynamics analysis

In order to understand the iodine adsorption behavior of γ-CD-MOFs, the experimental data were processed by pseudo-first-order kinetic model, pseudo-second-order kinetic model and intraparticle diffusion model, which can be expressed as follows [29–33]:

$$\ln\left(q_e - q_t\right) = \ln q_e - k_1 t \tag{4}$$

$$\frac{t}{q_t} = \frac{1}{k_2 q_e^2} + \frac{t}{q_e} \tag{5}$$

$$q_t = k_i t^{1/2} + C \tag{6}$$

where q_t (mg/g) and q_e (mg/g) represent the amounts of the iodine adsorbed (mg/g) at various time and equilibrium time, respectively; k_1 (h^{-1}) and k_2 ((g/mg/h) represent the kinetic rate constants for the pseudo-first-order and the pseudo-second-order models, respectively; k_i (mg/g/$h^{1/2}$) represents the intraparticle diffusion rate constant, and C (mg/g) represents the intercept which is in the direct ratio to the extent of boundary layer thickness.

The pseudo-first-order and pseudo-second-order curve-fittings are shown in Figs. 7(a) and (b), respectively. We were told from the parameters tabulated in Table 1 that the linear regression coefficient values of pseudo-second-order kinetic model (0.99, 0.99, 0.99, 0.99 and 0.99) are much higher than those of pseudo-first-order kinetic model (0.96, 0.96, 0.95, 0.93 and 0.93). Moreover, the practical value of q_e calculated from the pseudo-second-order kinetic model also got much closer to the theoretical value compared with that of the pseudo-first-order. These results indicated that the adsorption is dominated by the pseudo-second-order kinetic model which used to describe the chemisorption-type process effectively, and further confirmed the assumption of strong interaction between the γ-CD-MOFs and the iodine molecules. As shown in Fig. 7(c), the multilinear plots of q_t against $t^{1/2}$ suggested that the adsorption process involve two stages including the surface diffusion and the intraparticle diffusion, briefly, the intraparticle diffusion is not the only rate-determining step in the adsorption process (Table 2) [34].

3.2.4. Adsorption isotherms analysis

To further understand the adsorption mechanism and obtain the saturated adsorption capacity of iodine by the γ-CD-MOFs, batch experiments were conducted under three constant temperatures of 288, 298 and 308 K with different initial iodine concentrations. The most popular adsorption isothermal models were so-called Langmuir isotherm and Freundlich isotherm. The Langmuir sorption isotherm based on several basic assumptions is often applied for the monolayer adsorption process. In contrast, the adsorption isotherm model proposed by Freundlich, is usually used to analyze the multilayer adsorption.

The Langmuir isotherm model and the Freundlich isotherm model can be represented as follows [35–38]:

$$\frac{C_e}{q_e} = \frac{1}{K_L} + \frac{a_L C_e}{K_L} \tag{7}$$

$$\ln q_e = \ln K_F + \frac{1}{n} \ln c_e \tag{8}$$

where q_e (mg/g) represents the equilibrium adsorption capacity; C_e (mg/L) represents the iodine concentration at adsorption equilibrium; and K_L and a_L represent the Langmuir adsorption isotherm constants; K_F and n represent the Freundlich adsorption isotherm constants.

From Figs. 8(a)–(c), the adsorption performances of γ-CD-MOFs interpreted by the Langmuir and Freundlich models are clearly shown. The parameters (q_m, K_L, K_F, R_L, n and R^2) calculated based on each model are listed in Table 3 and 4, respectively. By comparing the linear correlation coefficient values of R^2, we can draw a conclusion that the Langmuir adsorption isotherm model describes the iodine adsorption process of γ-CD-MOFs better than the Freundlich adsorption isotherm model. This illustrated that the iodine adsorption by γ-CD-MOFs is a monolayer adsorption, which often occurs in the chemical adsorption or adsorption of microporous materials according to the previous literature. Furthermore, the maximum adsorption capacity of iodine by γ-CD-MOFs based on the Langmuir model was as high as 444.71, 449.71 and 460.59 mg/g at 288, 298 and 308 K, respectively.

Additionally, the separation factor "R_L", which is called equilibrium parameter, can be used to describe the fundamental characteristic of the Langmuir isotherm using the following equation [39]:

$$R_L = \frac{1}{1 + a_L C_0} \tag{9}$$

where C_0 (mg/L) presents the initial concentration and a_L (L/mg) presents the Langmuir constant. The value of R_L can be used to predict the shape of the adsorption isotherm: Unfavorable ($R_L > 1$), Linear ($R_L = 1$), Favorable ($0 < R_L < 1$) or Irreversible ($R_L = 0$).

As shown in Fig. 8(d), the R_L values for the iodine adsorption by γ-CD-MOFs at the temperatures of 288, 298 and 308 K were calculated to be in the ranges of 0.034–0.313, 0.027–0.312 and 0.018–0.191, respectively. These values suggested the favorable and endothermal nature of iodine adsorption by γ-CD-MOFs. The changes in the R_L values with the iodine concentration indicated that the low concentration of adsorption was more advantageous.

3.2.5. Adsorption mechanism

To make a long story short, we speculated the mechanisms of the iodine adsorption onto the γ-CD-MOFs may be attributed to a combination of perforated porousness and charge-transfer interactions. First, the porous networks of γ-CD-MOFs provided a free and easy access for the guest iodine molecules to accomplish the external diffusion and internal diffusion; then, the hydroxy-rich units presented a number of active binding sites for achieving the adsorption of iodine via host–guest interaction.

3.2.6. Adsorption thermodynamics analysis

The mechanism of iodine adsorption by γ-CD-MOFs can be explained by some basic thermodynamic parameters, such as Gibbs free energy ΔG (KJ/mol), enthalpy ΔH (KJ/mol) and entropy ΔS (J/mol/K), which can be expressed as follows [40]:

$$K_d = \frac{q_e}{c_e} \tag{10}$$

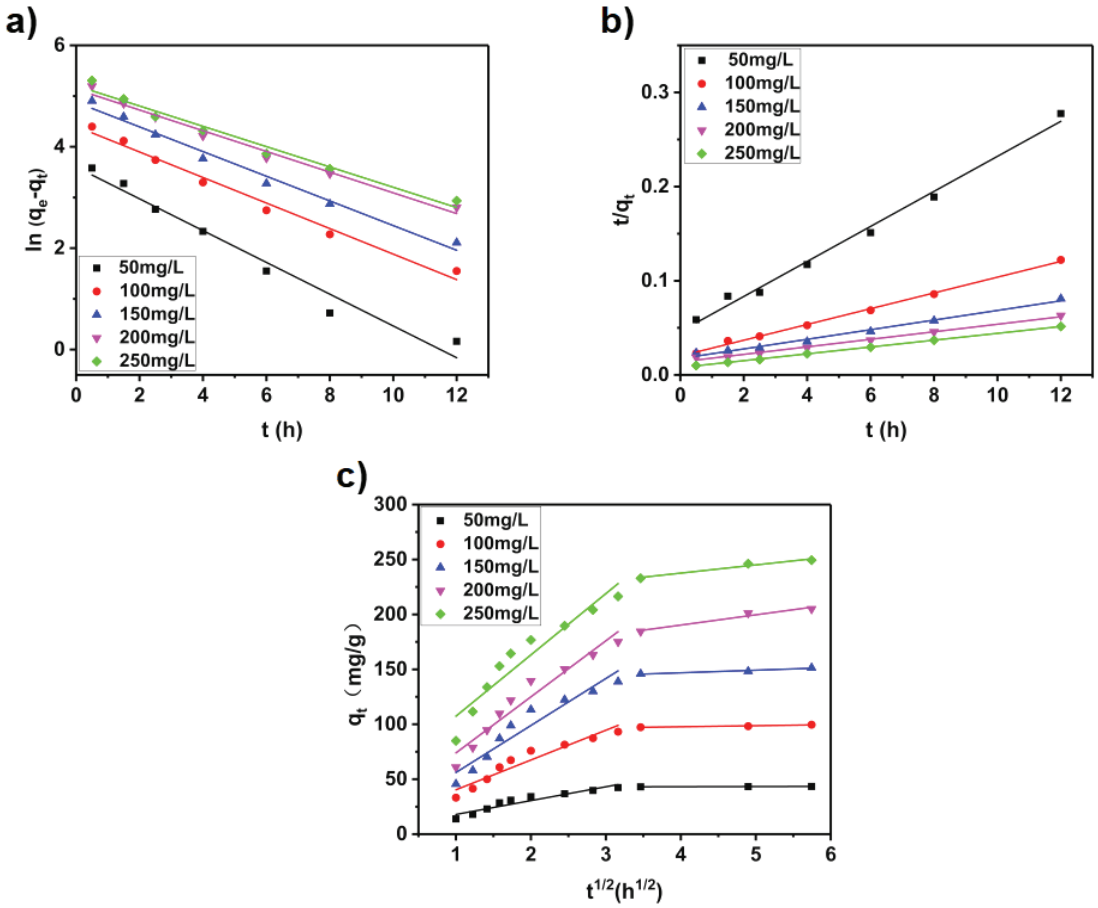

Fig. 7. (a) Pseudo-first-order curve-fittings, (b) pseudo-second-order curve-fittings and (c) intraparticle diffusion models for iodine adsorption by γ-CD-MOFs at different initial iodine concentrations.

Table 1
Kinetic parameters of iodine adsorption by γ-CD-MOFs

C_0 (mg/L)	$q_{e,exp}$ (mg/g)	Pseudo-first-order kinetics			Pseudo-second-order kinetics		
		k_1 (h^{-1})	$q_{e,cal}$ (mg/g)	R^2	k_2 (g/mg/h)	$q_{e,cal}$ (mg/g)	R^2
50	42.35	0.48	50.77	0.96	0.020	49.16	0.99
100	93.24	0.20	70.71	0.96	0.009	112.74	0.99
150	138.80	0.19	111.89	0.95	0.006	175.49	0.99
200	175.00	0.15	144.24	0.93	0.004	227.79	0.99
250	216.50	0.16	161.01	0.93	0.004	268.10	0.99

Table 2
Intraparticle diffusion model parameters for the adsorption of iodine by γ-CD-MOFs

C_0 (mg/L)	Intraparticle diffusion model					
	$k_{i,1}$ (mg/g/$h^{1/2}$)	C_1 (mg/g)	R^2	$k_{i,2}$ (mg/g/$h^{1/2}$)	C_2 (mg/g)	R^2
50	12.59	5.34	0.91	0.14	42.59	0.96
100	27.11	13.26	0.92	0.95	93.92	0.93
150	42.77	13.36	0.92	2.35	137.45	0.95
200	51.03	22.93	0.94	9.31	153.08	0.96
250	55.79	51.59	0.91	7.43	207.88	0.96

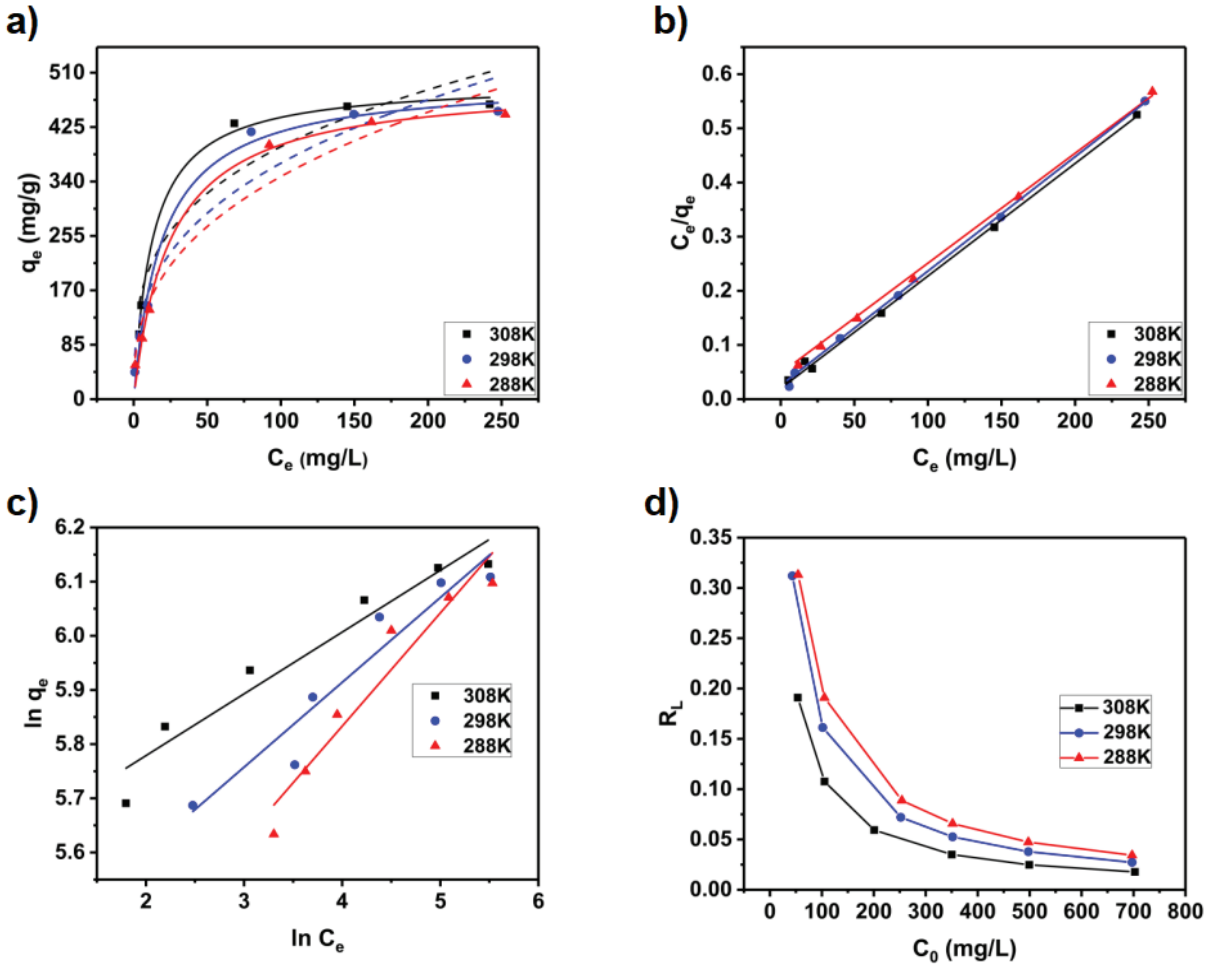

Fig. 8. (a) Data fitting with Langmuir and Freundlich adsorption isotherms of iodine adsorption by γ-CD-MOFs at different temperatures (288, 298 and 308 K); solid lines: Langmuir model, dashed lines: Freundlich model. (b) and (c) are the Langmuir and Freundlich linear fittings for the iodine adsorption by γ-CD-MOFs, respectively. (d) Separation factor for iodine adsorption by γ-CD-MOFs.

Table 3
Langmuir isotherm parameters for iodine adsorption by γ-CD-MOFs

Langmuir isotherm	Temperature (K)	Q_m	K_L	R^2	R_L
L	288	444.71	0.04	0.99	0.034~0.313
	298	449.71	0.05	0.99	0.027~0.312
	308	460.59	0.08	0.99	0.018~0.191

Table 4
Freundlich isotherm parameters for iodine adsorption by γ-CD-MOFs

Freundlich isotherm	Temperature (K)	K_F	R^2	1/n
F	288	64.19	0.95	0.37
	298	75.77	0.92	0.34
	308	101.85	0.90	0.29

$$\Delta G = -RT\ln\left(K_d\right) \tag{11}$$

$$\ln\left(K_d\right) = \frac{\Delta S}{R} - \frac{\Delta H}{RT} \tag{12}$$

where K_d (L/g) presents the distribution coefficient defined by q_e/C_e; R (8.314 J/mol/K) presents the universal gas constant and T (K) presents the temperature.

The obtained Gibbs free energy (ΔG), adsorption enthalpy (ΔH) and entropy (ΔS) of iodine adsorption by γ-CD-MOFs at three temperatures are listed in Table 5. The calculated ΔG values were varied in the ranges of –7.11 to –8.50KJ/mol , –6.57 to –8.12 KJ/mol, –5.45 to –5.96 KJ/mol, –3.86 to –4.69 KJ/mol and –1.45 to –2.49 KJ/mol at different initial iodine concentrations under three temperatures, respectively (Fig. 9). In view of the negative values of ΔG, it is very sensitive, the iodine adsorption by γ-CD-MOFs were spontaneous and endothermic. Furthermore, the enthalpy ΔH and

Table 5
Thermodynamic parameters of iodine adsorption by γ-CD-MOFs

C_0 (mg/L)	ΔG (KJ/mol)			ΔH (KJ/mol)	ΔS (KJ/mol/K)
	288 K	298 K	308 K		
100	–7.11	–8.01	–8.50	20.05	0.093
150	–6.57	–6.98	–8.12	22.24	0.099
350	–5.45	–5.75	–5.96	7.36	0.043
500	–3.86	–4.24	–4.69	11.85	0.054
700	–1.45	–1.53	–2.49	14.81	0.056

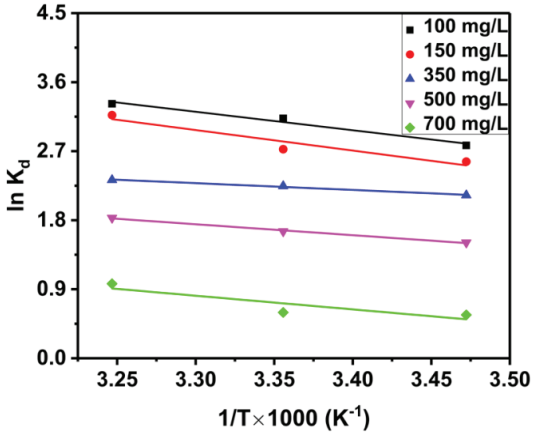

Fig. 9. Van't Hoff plots to get the ΔH and ΔS of iodine adsorption by γ-CD-MOFs.

the entropy ΔS at different concentrations could be calculated from the slopes and intercepts of the linear plots of ln K_d vs. 1/T to be 20.05 KJ/mol and 0.093 KJ/mol/K, 22.24 KJ/mol and 0.099 KJ/mol/K, 7.36 KJ/mol and 0.043 KJ/mol/K, 11.85 KJ/mol and 0.054 KJ/mol/K, 14.81 KJ/mol and 0.056 KJ/mol/K, respectively. Likewise, the positive values of ΔH and ΔS at all temperatures demonstrated the iodine adsorption by γ-CD-MOFs were spontaneous and endothermic once again [41,42].

4. Conclusion

To sum up, the γ-CD-MOFs with large cavities, high specific surface areas and a great deal of hydroxyl functional groups were proved to be a kind of good candidate for iodine capture and adsorption. In this study, under optimal conditions of concentration 50 mg/L, γ-CD-MOFs dosage 1 g/L and contact time 12 h, the removal efficiency was up to 100%. Moreover, the maximum gas iodine uptake of 104 wt% was obtained, whereby the maximum adsorption capacity of γ-CD-MOFs was up to 449.71 mg/g at 298 K. This lays a foundation for the porous MOFs to replace traditional porous materials applied for remediation of radioactive iodine with broad prospect promotion.

Acknowledgments

This work was supported by the National Natural Science Foundation of China (Project No. 21601177 and 41772241) and the 111 Project (B16020).

References

[1] H. Ma, J.J. Chen, L. Tan, J.H. Bu, Y. Zhu, B. Tan, C. Zhang, Nitrogen-rich triptycene-based porous polymer for gas storage and iodine enrichment, ACS. Macro. Lett., 5 (2016) 1039–1043.
[2] K. Kosaka, M. Asami, N. Kobashigawa, K. Ohkubo, H. Terada, N. Kishida, M. Akiba, Removal of radioactive iodine and cesium in water purification processes after an explosion at a nuclear power plant due to the Great East Japan earthquake, Water. Res., 46 (2012) 4397–4404.
[3] X. Qian, Z.Q. Zhu, H.X. Sun, F. Ren, P. Mu, W.D. Liang, L.H. Chen, A. Li, Capture and reversible storage of volatile iodine by novel conjugated microporous polymers containing thiophene units, ACS. Appl. Mater. Interfaces, 8 (2016) 21063–21069.
[4] L. Lin, H. Guan, D. Zou, Z. Dong, Z. Liu, F. Xu, Z. Xie, Y. Li, A pharmaceutical hydrogen-bonded covalent organic polymer for enrichment of volatile iodine, RSC. Adv., 7 (2017) 54407–54415.
[5] X.Y. Zhang, P. Gu, X.Y. Li, G.H. Zhang, Efficient adsorption of radioactive iodide ion from simulated wastewater by nano Cu_2O/Cu modified activated carbon, Chem. Eng. J., 322 (2017) 129–139.
[6] C.P.J. Isaac, A. Sivakumar, Removal of lead and cadmium ions from water using Annona squamosa shell: kinetic and equilibrium studies, Desal. Wat. Treat., 51 (2013) 7700–7709.
[7] H. Li, X.S. Ding, B.H. Han, Porous azo-bridged porphyrin-phthalocyanine network with high iodine capture capability, Chem. Eur. J., 22 (2016) 11863–11868.
[8] I. Ali, New generation adsorbents for water treatment, Chem. Rev., 112 (2012) 5073–5091.
[9] A. Sigen, Y. Zhang, Z. Li, H. Xia, M. Xue, X. Liu, Y. Mu, Highly efficient and reversible iodine capture using a metalloporphyrin-based conjugated microporous polymer, Chem. Commun., 50 (2014) 8495–8498.
[10] A. Schneemann, V. Bon, I. Schwedler, I. Senkovska, S. Kaskel, R.A. Fischer, Flexible metal-organic frameworks, Chem. Soc. Rev., 43 (2014) 6062–6096.
[11] A. Schaate, P. Roy, A. Godt, J. Lippke, F. Waltz, M. Wiebcke, P. Behrens, Modulated synthesis of Zr-based metal-organic frameworks: from nano to single crystals, Chem. Eur. J., 17 (2011) 6643–6651.
[12] X. Zhou. Y. Zhu. L. Li. T. Yang. J. Wang, W. Huang, Lanthanide-organic frameworks based on terphenyl-tetracarboxylate ligands: syntheses, structures, optical properties and selective sensing of nitro explosives, Sci. China. Chem., 60 (2017) 1130–1135.
[13] J.R. Long, O.M. Yaghi, The pervasive chemistry of metal-organic frameworks, Chem. Soc. Rev., 38 (2009) 1213–1214.
[14] E. Hadinejad, S. Hashemian, S.A. Yasini, Comparison of catalytic effect of Fe- MOF and Fe-ZIF for Fenton degradation of Eriochrom black T, Desal. Wat. Treat., 90 (2017) 180–188.
[15] Alireza Behvandi, Farhad Khorasheh, Ali Akbar Safekordi, Adsorption of terephthalic acid and p-toluic acid from aqueous solution using metal organic frameworks: effect of molecular properties of the adsorbates and structural characteristics of the adsorbents, Desal. Wat. Treat., 66 (2017) 367–382.
[16] K.Y. Jee, J.S. Kim, J. Kim, Y.T. Lee, Effect of hydrophilic $Cu_3(BTC)_2$ additives on the performance of PVDF membranes for water flux improvement, Desal. Wat. Treat., 57 (2016) 17637–17645.
[17] L. Li, L.J. Yuan, W. Hong, L. Fan, L.B. Mao, L. Liu, Hybrid Fe_3O_4/MOFs for the adsorption of methylene blue and methyl violet from aqueous solution, Desal. Wat. Treat., 55 (2015) 1973–1980.
[18] K. Xie, C.H. Shan, J.S. Qi, S. Qiao, Q.S. Zeng, L.Y. Zhang, Study of adsorptive removal of phenol by MOF-5, Desal. Wat. Treat., 54 (2015) 654–659.
[19] Z. Hasan, S.H. Jhung, Removal of hazardous organics from water using metal-organic frameworks (MOFs): plausible mechanisms for selective adsorptions, J. Hazard. Mater., 283 (2015) 329–339.
[20] B. Liu, H. Li, X. Xu, X. Li, N. Lv, V. Singh, J.F. Stoddart, P. York, X. Xu, R. Gref, J. Zhang, Optimized synthesis and crystalline stability of γ-cyclodextrin metal-organic frameworks for drug adsorption, Int. J. Pharm., 514 (2016) 212–219.

[21] Z. Moussa. M. Hmadeh. M.G. Abiad. O.H. Dib, D. Patra, Encapsulation of curcumin in cyclodextrin-metal organic frameworks: dissociation of loaded CD-MOFs enhances stability of curcumin, Food. Chem., 212 (2016) 485–494.
[22] X. Xu, C. Wang, H. Li, L. Xue, B. Liu, V. Singh, S. Wang, L. Sun, R. Gref, J. Zhang, Evaluation of drug loading capabilities of γ-cyclodextrin-metal organic frameworks by high performance liquid chromatography, J. Chromatogr. A, 1488 (2017) 37–44.
[23] X. Li, T. Guo, L. Lachmanski, F. Manoli, M. Menendezmiranda, I. Manet, Z. Guo, L. Wu, J. Zhang, R. Gref, Cyclodextrin-based metal-organic frameworks particles as efficient carriers for lansoprazole: study of morphology and chemical composition of individual particles, Int. J. Pharm., 531 (2017) 424–432.
[24] R.A. Smaldone, R.S. Forgan, H. Furukawa, J.J. Gassensmith, A.M.Z. Slawin, O.M. Yaghi, J.F. Stoddart, Metal-organic frameworks from edible natural products, Angew. Chem. Int. Ed. Engl., 49 (2010) 8630–8634.
[25] Y. Furukawa, T. Ishiwata, K. Sugikawa, K. Kokado, K. Sada, Nano- and microsized cubic gel particles from cyclodextrin metal-organic frameworks, Angew. Chem. Int. Ed. Engl., 51 (2012) 10566–10569.
[26] J.M. Duan, B. Su, Removal characteristics of Cd(II) from acidic aqueous solution by modified steel-making slag, Chem. Eng. J., 246 (2014) 160–167.
[27] Y. Liao, J. Weber, B.M. Mills, Z. Ren, C.F.J. Faul, Highly efficient and reversible iodine capture in hexaphenylbenzene-based conjugated microporous polymers, Macromolecules, 49 (2016) 6322–6333.
[28] T. Hasell, M. Schmidtmann, A.I. Cooper, Molecular doping of porous organic cages, J. Am. Chem. Soc., 133 (2011) 14920–14923.
[29] J. Dong, F.F. Xu, Z.J. Dong, Y.S. Zhao, Y. Yan, H. Jin, Y.X. Li, Fabrication of two dual-functionalized covalent organic polymers through heterostructural mixed linkers and their use as cationic dye adsorbents, RSC. Adv., 8 (2018) 19075–19084.
[30] Y.S. Ho, G. McKay, Pseudo-second order model for sorption processes, Process. Biochem., 34 (1999) 451–465.
[31] S.X. Duan, R.F. Tang, Z.C. Xue, X.X. Zhang, Y.Y. Zhao, W. Zhang, J.H. Zhang, B.Q. Wang, S.Y. Zeng, D.Z. Sun, Effective removal of Pb(II) using magnetic $Co_{0.6}Fe_{2.4}O_4$ micro-particles as the adsorbent: synthesis and study on the kinetic and thermodynamic behaviors for its adsorption, Colloids. Surf. A., 469 (2015) 211–223.
[32] D. Balarak, F. Mostafapour, E. Bazrafshan, T.A. Saleh, Studies on the adsorption of amoxicillin on multi-wall carbon nanotubes, Water. Sci. Technol., 75 (2017) 1599–1606.
[33] D. Balarak, H. Azarpira, F.K. Mostafapour, Study of the adsorption mechanisms of cephalexin on to azolla filiculoides, Der. Pharma. Chemica., 8 (2016) 114–121.
[34] Y. Li, Q. Du, T. Liu, J. Sun, Y. Jiao, Y. Xia, L. Xia, Z. Wang, W. Zhang, K. Wang, Equilibrium, kinetic and thermodynamic studies on the adsorption of phenol onto graphene, Mater. Res. Bull., 47 (2012) 1898–1904.
[35] I. Langmuir, The adsorption of gases on plane surfaces of glass, mica and platinum, J. Am. Chem. Soc., 40 (1918) 1361–1403.
[36] H. Freundlich, W. Heller, The adsorption of cis- and trans-azobenzene, J. Am. Chem. Soc., 61 (1939) 2228–2230.
[37] S. Ahmadi, A. Banach, F.K. Mostafapour, D. Balarak, Study survey of cupric oxide nanoparticles in removal efficiency of ciprofloxacin antibiotic from aqueous solution: adsorption isotherm study, Desal. Wat. Treat., 89 (2017) 297–303.
[38] D. Balarak, F.K. Mostafapour, H. Azarpira, Adsorption isotherm studies of tetracycline antibiotics from aqueous solutions by maize stalks as a cheap biosorbent, Int. J. Pharm. Tech., 8 (2016) 16664–16675.
[39] D.D. Lu, Q.L. Cao, X.J. Cao, F. Luo, Removal of Pb(II) using the modified lawny grass: mechanism, kinetics, equilibrium and thermodynamic studies, J. Hazard. Mater., 166 (2009) 239–247.
[40] Y.J. Yao, S.D. Miao, S.M. Yu, L.P. Ma, H.Q. Sun, S.B. Wang, Fabrication of Fe_3O_4/SiO_2 core/shell nanoparticles attached to graphene oxide and its use as an adsorbent, J. Colloid. Interface. Sci., 379 (2012) 20–26.
[41] M. Kara, H. Yuzer, E. Sabah, M.S. Celik, Adsorption of cobalt from aqueous solutions onto sepiolite, Water. Res., 37 (2003) 224–232.
[42] Q.X. Yang, Q.Q. Zhao, S.S. Ren, Z.J. Chen, H.G. Zheng, Assembly of Zr-MOF crystals onto magnetic beads as a highly adsorbent for recycling nitrophenol, Chem. Eng. J., 323 (2017) 74–83.
[43] B.J. Riley, J. Chun, J.V. Ryan, J. Matyáš, X.S. Li, D.W. Matson, S.K. Sundaram, D.M. Strachan, J.D. Vienna, Chalcogen-based aerogels as a multifunctional platform for remediation of radioactive iodine, RSC. Adv., 1 (2011) 1704–1715.
[44] B.F. Abrahams, M. Moylan, S.D. Orchard, R. Robson, Zinc saccharate: a robust, 3D coordination cetwork with two types of isolated, parallel channels, one hydrophilic and the other hydrophobic, Angew. Chem. Int. Ed. Engl., 42 (2003) 1848–1851.
[45] A.P. Katsoulidis, J.Q. He, M.G. Kanatzidis, Functional monolithic polymeric organic framework aerogel as reducing and hosting media for Ag nanoparticles and application in capturing of Iodine Vapors, Chem. Mater., 24 (2012) 1937–1943.
[46] K.W. Chapman, P.J. Chupas, T.M. Nenoff, Radioactive iodine capture in silver-containing mordenites through nanoscale silver iodide formation, J. Am. Chem. Soc., 132 (2010) 8897–8899.
[47] Q.K. Liu, J.P. Ma, Y.B. Dong, Highly efficient iodine species enriching and guest-driven tunable luminescent properties based on a cadmium(II)-triazole MOF, Chem. Commun. (Camb)., 47 (2011) 7185–7187.
[48] Y.F. Chen, H.X. Sun, R.X. Yang, T.T. Wang, C.J. Pei, Z.T. Xiang, Z.Q. Zhu, W.D. Liang, A. Li, W.Q. Deng, Synthesis of conjugated microporous polymer nanotubes with large surface areas as absorbents for iodine and CO_2 uptake, J. Mater. Chem. A, 3 (2015) 87–91.
[49] D.F. Sava, T.J. Garino, T.M. Nenoff, Iodine confinement into metal-organic frameworks (MOFs): low-temperature sintering glasses to form novel glass composite material (GCM) alternative waste forms, Ind. Eng. Chem. Res., 51 (2012) 614–620.
[50] K.C. Park, J. Cho, C.Y. Lee, Porphyrin and pyrene-based conjugated microporous polymer for efficient sequestration of CO_2 and iodine and photosensitization for singlet oxygen generation, RSC. Adv., 6 (2016) 75478–75481.
[51] C. Pei, T. Ben, S. Xu, S.J. Qiu, Ultrahigh iodine adsorption in porous organic frameworks, Mater. Chem. A, 2 (2014) 7179–7187.
[52] Y. Li, W.B. Chen, W.J. Hao, Y.S. Li, L. Chen, Covalent organic frameworks constructed from flexible building blocks with high adsorption capacity for pollutants, ACS. Appl. Nano. Mater., 1 (2018) 4756–4761.

Supporting information

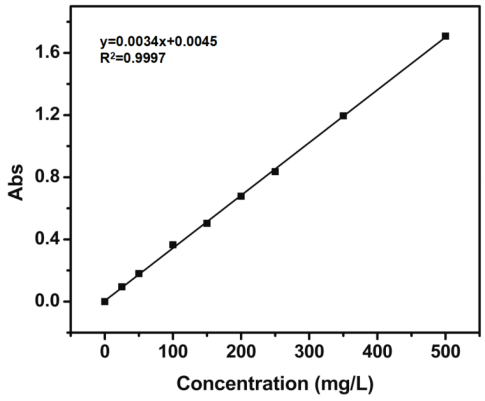

Fig. S1. Calibration plot of standard iodine in hexane solutions obtained by UV-Vis spectrophotometer at 525 nm.

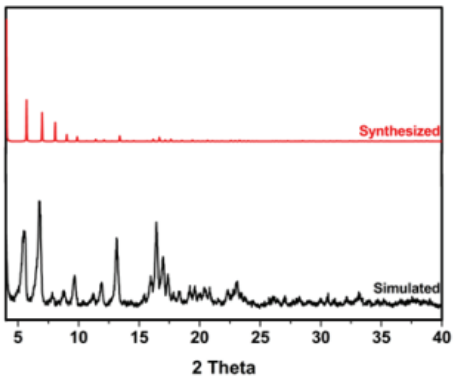

Fig. S2. PXRD spectra of simulated and synthesized γ-CD-MOFs.

Table S1
Comparison of the maximum adsorption capacity of iodine on different adsorbents

No.	Adsorbents	Temperature (°C)	Adsorbent capacity (mg/g)	References
1	Activated carbon	75	30	[1]
2	Cg-5P	~25	87	[43]
3	$[Zn(C_6H_8O_8)]\cdot\approx 2H_2O$	19	166	[44]
4	Ag@Mon-POF	70	250	[45]
5	Ag@Zeolite Mordenites	95	275	[46]
6	CC3	~20	364	[28]
7	$[Cd(L)_2(ClO_4)_2]\cdot H_2O$	~25	~460	[47]
8	CMPN-1	70	970	[48]
9	γ-CD-MOF	80	~1,040	This work
10	CMPN-2	70	1,100	[48]
11	ZIF-8	75	1,200	[49]
12	Por-Py-CMP	77	1,300	[50]
13	PAF-1	25	1,440	[51]
14	HCMP-1	85	1,590	[52]
15	CMPN-3	70	2,080	[48]